CHINESE OPTICS LETTERS

Vol. 21, No. 10 | October 2023

Review of advanced progress of χ^2-based all-optical devices on thin-film lithium niobate

Lei Shi (石 磊)[1,†], Yuanjun Song (宋元军)[1,†], Jie Tang (唐 杰)[2,3], Yanyan Qin (秦妍妍)[1], Xiaomei Xue (薛小枚)[4], Huanli Zhou (周桓立)[1], Zexian Chen (陈泽贤)[1], Xuan Li (李 选)[1], Guang Qian (钱 广)[2,3], Xiaoyang Zhang (张晓阳)[1,5], and Tong Zhang (张 彤)[1,4,5*]

[1] Joint International Research Laboratory of Information Display and Visualization, School of Electronic Science and Engineering, Southeast University, Nanjing 210096, China

[2] National Key Laboratory of Solid-State Microwave Devices and Circuits, Nanjing 210016, China

[3] Nanjing Electronic Devices Institute, Nanjing 210016, China

[4] Key Laboratory of Micro-Inertial Instrument and Advanced Navigation Technology, Ministry of Education, and School of Instrument Science and Engineering, Southeast University, Nanjing 210096, China

[5] Suzhou Key Laboratory of Metal Nano-Optoelectronic Technology, Southeast University Suzhou Campus, Suzhou 215123, China

*Corresponding author: tzhang@seu.edu.cn

Received April 17, 2023 | Accepted June 9, 2023 | Posted Online October 10, 2023

The technological innovation of thin-film lithium niobate (TFLN) is supplanting the traditional lithium niobate industry and generating a vast array of ultra-compact and low-loss optical waveguide devices, providing an unprecedented prospect for chip-scale integrated optics. Because of its unique strong quadratic nonlinearity, TFLN is widely used to create new coherent light, which significantly promotes all-optical signal processes, especially in terms of speed. Herein, we review recent advances in TFLN, review the thorough optimization strategies of all-optical devices with unique characteristics based on TFLN, and discuss the challenges and perspectives of the developed nonlinear devices.

Keywords: thin-film lithium niobate; second-order nonlinearity; nonlinear integrated optics.
DOI: 10.3788/COL202321.101901

1. Introduction

Integrated optics with cheap, high efficiency, low-pump, and large-scale integration will prevail in the future. This includes various functional integrated optical devices on a single substrate, which show significant potential in applications in many optical fields, such as optical interconnection[1], optical communication[2,3], quantum computing[4,5], optical neural network computing[6], and sensing systems[7]. In integrated optics, the nonlinear property provides novel applications with its extreme spectral broadening and optical signal processing capability. This effect has become an intriguing element for various applications, including a source of coherent infrared light[8], photon-pair generation[9], frequency conversion[10], low-threshold optical parametric oscillators[11], and generation of the terahertz wave[12]. Many second-order nonlinear materials, including lithium niobate (LN, nonlinear coefficient $d_{33} \approx 25\,\mathrm{pm/V}$)[13], gallium arsenide (GaAs, $d_{36} \approx 119\,\mathrm{pm/V}$)[13], and aluminum nitride (AlN, $d_{33} \approx 4.7\,\mathrm{pm/V}$)[14] have been adopted in nonlinear optical effects. Among them, LN is widely used for various applications in integrated optical platforms for its excellent electro-optic, nonlinearity, piezoelectric, and acousto-optic properties[15]. Although GaAs shows stronger nonlinearity than LN, it is not a ferroelectric material, and the lack of flexible phase matching schemes limits its application in frequency conversion. Hence, leveraging the sufficiently high nonlinear properties of having an ultra-wide transparent window (range from 0.4 to 5 μm), piezoelectric and pyroelectric, LN has provided fascinating and flexible platforms for nonlinear optics.

Despite its considerable potential, LN has encountered a bottleneck in integrated optical platforms compared with other competitive platforms mainly due to the unique complicatedness of its material manufacture and integration. The traditional LN device was fabricated by titanium (Ti) diffusion or by anneal proton exchange of an LN crystal[16–19]. However, the refractive index distribution of the diffusion LN waveguide fabricated by the above technology is of the gradual type. For such LN waveguides, only the weak-guiding waveguide with a low refractive index difference can reduce the transmission loss of the waveguide. Although it can broaden bandwidth by imposing resonators, its subtle contrast of index ($\Delta n \approx 0.01$)[19,20] leads to weak mode confinement, large cross-section, and small optical overlap, which causes a significant loss of light[21]. Moreover, this

technology will produce a photo-induced effect that causes large refractive-index nonuniformity[22]. These problems impede the miniaturization and monolithic integration of traditional LN optical devices.

Recently, high-quality thin-film lithium niobate (TFLN), fabricated using the intelligent "ion slicing" technique, can miniaturize the integrated optics while preserving the material's original properties. The "ion slicing" technique was introduced by Levy *et al.* in 1998 when a 9-μm-thick wafer was separated, and its properties were maintained as a single-crystal bulk[23]. The LN crystal dosing He^+ ions was bonded to a pre-grown low-index substrate (e.g., SiO_2). After being heated at a specific temperature, the TFLN was exfoliated, which retained the properties of the LN crystal. Detailed processes of the TFLN technology can be referred to in relevant references[15,24–27]. Hence, a promising configuration guided by silicon-on-insulator technology, called the LN-on-insulator (TFLN) technique, generated revolutionary progress in the magnitude of sub-micrometer fabrication of LN integrated optical devices using "ion slicing and wafer bonding" technique[24]. Based on this technique, it is reported that NANOLN Inc. has commercialized the results of its high-quality TFLN substrate, which has extensively promoted the application research of integrated photonics on the TFLN platform and enhanced the commercial value of LN[28]. With the configuration, a much increased index contrast ($\Delta n > 0.6$)[25] exists between LN and air or the silica buffer layer so that the thin-film waveguide would firmly guide the planar waveguide. Hence, the tight spatial confinement found in TFLN devices increases the field intensity 20-fold relative to diffused waveguides[10,21,29]. However, the thicker the film is, the more propagation modes of light are allowed, which hinders the integration of nonlinear optical chips. Up to now, TFLN has reached the thickness of the submicron scale (range from 300 nm to 900 nm)[24,27], having the great characteristics of low-pump, high-gain, high-conversion-efficiency, and ultra-low-loss integrated nonlinear optical devices. In particular, periodically poled lithium niobate (PPLN) thin film is commonly used in wave mixing for all-optical signal processing. It is worth noting that all-optical signal processing is not limited to χ^2-based nonlinear effect. However, this review will focus on the χ^2-based nonlinear process because of its strong nonlinearity of TFLN.

Wave mixing encompasses the intrinsic all-optical interaction in the media with a unique, effective nonlinear metric, which exhibits far superior performance when compared with the process of electron transmission. Hence, this wave mixing based on the all-optical phenomena created a collection of new potentials (e.g., a broad bandwidth in the THz range[30,31], an active operation switch[32], and all-optical computing[33]). Notwithstanding, all-optical nonlinear devices based on TFLN are still in their infancy. Therefore, people continue to pursue higher-quality optical confinement devices and optimize the preparation process of materials. On the other hand, the innovation of properties can be constantly explored and gradually applied to the market through the innovative design of the device structure. The performance of versatile all-optical nonlinear devices has been verified experimentally, showing great potential and development opportunities in integrated nonlinear optics. With such a strong nonlinearity and light constraint capability, we expect TFLN to become a material platform of choice for realizing high-performance nonlinear optical devices.

Before this, many reviews of integrated nonlinear optics based on TFLN were mainly classified by different ways of wave interaction[15,34–38]. In this review, to clarify the recent development of all-optical nonlinear devices based on TFLN, we discuss the characteristics of versatile devices by focusing on their different roles in optical circuits. Further, this paper provides the route for optimizing the unique property of optical elements in the LN platform. The reviewed construction blocks are wavelength converters (Section 2), optical parametric amplifiers (Section 3), optical parametric oscillators (Section 4), optical frequency combs (Section 5), and optical switches (Section 6). Finally, we summarize the status of all the applications, emphasizing the remaining challenges and the distinctive perspectives that could transfer the device from the lab to the broader field.

2. Wavelength Converters in Wave Optics

The all-optical wavelength converter is a critical device used in the construction of a high-speed and non-blocking wavelength-division multiplexing (WDM) network since it can satisfy the mass transmission of information under the conditions of the wavelength of light, leading to the enhancement of reconfigurability, flexibility, and transmission efficiency in solving channel competition issues and improving wavelength utilization. Hence, based on various nonlinear processes, the wavelength converter is designed to achieve high conversion efficiency under pumping conditions with continuous or pulsed lasers. Thus far, second-harmonic generation, called SHG, is the predominant strategy that has been well developed in wavelength converters. Therefore, in this review, we mainly focus on the discussion of wavelength conversion based on second-harmonic generation in Section 2.1. Other nonlinear effects, such as sum frequency generation (SFG) and difference frequency generation (DFG), will be briefly discussed in Section 2.2.

2.1. Second-harmonic generation with wavelength conversion

The procedure of second-harmonic generation (SHG), in which a medium with nonzero second-order susceptibility χ^2 radiates a new wave at the double frequency 2ω when the intense pump laser was introduced. The second harmonic (~347 nm) was first observed experimentally in 1963 by focusing a ruby laser beam on the front of the surface of a plate of crystalline quartz (F61)[39]. Thereafter, SHG became widely used in wavelength conversion for broadening the spectrum in bulk LN and other nonlinear media. Up to now, high-efficiency and wide-bandwidth wavelength converters are popular in the research[10,40,41]. Here, we will review the recent progress of the wavelength converter in TFLN.

2.1.1. High conversion efficiency

Compared with crystal, the most feasible way to reach a conversion efficiency (CE) nearing 100% is to use an LN waveguide, which can confine the optical field well. Thus, the optimization process in the design of an LN waveguide should be given more attention. With the relationship between the conversion efficiency and phase difference $\eta \propto \mathrm{sinc}^2(\Delta k \cdot L/2)/A_{\mathrm{eff}}$, the effective area A_{eff} can be concerned with quadratic nonlinearity, which shows one of the standards for the design of waveguides under the coupled mode theory[42]. In addition, efficient second-harmonic generation is also optimized via the phase matching (PM) method, which depends on energy and momentum conservation. The ideal PM could be realized in different ways, which includes the following: (1) for birefringence or intermodal PM, $\Delta k \cdot L = (2k_{\mathrm{FW}} - k_{\mathrm{SH}}) \cdot L = 0$, $k_i = \frac{n_{\mathrm{eff}}(\omega_i)\omega_i}{c}$ $(i = \mathrm{FW}, \mathrm{SH})$, where Δk denotes the wavevector mismatch, L denotes the propagation length, k_i denotes the wave vector, $n_{\mathrm{eff}}(\omega_i)$ denotes the effective index at a specific frequency, ω_i denotes the angular frequency, and c denotes the velocity of light; (2) for quasi phase matching (QPM), $\Delta k \cdot L = (2k_{\mathrm{FW}} - k_{\mathrm{SH}} - G) \cdot L = 0$, where $G = 2\pi/\Lambda$ is the reciprocal vector, and Λ is the poling period[43]. Under the ideal phase-matching condition, the energy can efficiently transfer from the pump light to the signal light when the wave propagates through the nonlinear medium with distance L. Meanwhile, the refractive index of the pump wave $n_{\mathrm{eff}}(\omega_p)$ and the signal wave $n_{\mathrm{eff}}(\omega_c)$ should satisfy with $n_{\mathrm{eff}}(\omega_p) = n_{\mathrm{eff}}(\omega_c)$ in the birefringence or the intermodal PM while in QPM, this condition should not be satisfied due to the compensation of the reciprocal vector G. Also, this condition should be concerned with the phase-matching process. As critical guidance of waveguide design, this phase-matching engineering was implemented by birefringent PM[44], intermodal PM[45], and QPM[40]. The variety of phase matching provides a versatile toolbox for the flexible design of devices. The essential parameters of design and performance are summarized in Table 1.

Birefringent crystals can achieve ideal PM by adjusting the temperature or cut direction of the crystal, which requires strict constrain over the polarization of different waves in different axes. As shown in Table 1, the birefringent PM was realized in an angle-cut LN waveguide where the light propagated in the direction with a certain angle ($\theta = 52°$) to the crystal axis[44]. Although birefringent PM can simplify the fabrication process by changing the angle and the temperature, different from the complex poling processes of the crystal, this led to a limited conversion efficiency of $2.7\%/(\mathrm{W} \cdot \mathrm{cm}^2)$. Meanwhile, since the light at both frequencies could not be simultaneously polarized on the

Table 1. Comparison of Different Wavelength Converters Based on the TFLN.

Type	Structure	Wafer Cut	Etch Depth (μm)	Length (mm)	CE [%/(W·cm2)]	Bandwidth (nm)	Year	Ref.
Birefringence	TFLN	Angle-cut	9	20	2.7	<4	2022	[44]
Intermodal	Polymer-TFLN	Z-cut	0.6 (polymer)	5	0.175	<4	2022	[46]
	Hybrid TFLN	Z-cut	–	2.5	4.05	<10	2022	[47]
	Grooved	X-cut	0.08	0.5	6.8	<10	2017	[48]
	TFLN	Z-cut	0.46	8	7.34	<4	2018	[49]
	Heterogeneous	X-cut	0.2	2.35	650	<4	2018	[50]
	TFLN	X-cut	0.57	1.2	5540	3	2021	[45]
QPM	SiN-PPLN	Y-cut	0.4 (SiN)	4.9	0.8	–	2017	[51]
	SiN-PPLN	X-cut	0.39 (SiN)	4.8	160	3	2016	[52]
	PPLN	Z-cut	2.5	20	320	0.5	2022	[53]
	PPLN	X-cut	0.34	6	1100	>110	2020	[54]
	PPLN	X-cut	~0.3	4	2600	<10	2018	[10]
	PPLN	Z-cut	0.375	6	2900	–	2021	[55]
	PPLN	X-cut	0.35	6	3061	4	2020	[56]
	PPLN	X-cut	0.05	7	3757	1	2020	[57]
	PPLN	X-cut	0.1	0.6	4600	14	2019	[21]
	PPLN	X-cut	0.1	4.2	33,000	<1	2021	[40]

anomalous axis, which led to the unavailability of a maximum nonlinear coefficient, the conversion efficiency of the converter was also greatly limited. However, the main reason for the low conversion efficiency of this work was the large size of the waveguide. If possible, then the conversion efficiency will be enhanced over 7000%/(W · cm^2) in a nanowaveguide with simulation.

In addition to birefringent PM, another phase matching method was also proposed. This method was called intermodal PM, which was typically realized via a couple of modes dispersion engineering with the fundamental and higher-order modes (see Table 1). That is to say, the lower-order mode of the fundamental wave should be matched with the higher-order mode of the second-harmonic wave in the case of the same polarization. This has been demonstrated in the studies of a ridge waveguide, which loads the stripe or grating in TFLN[46–48,50]. As one of the most traditional pathways, the intermodal PM suffers from field mismatch because of the symmetry profile between the fundamental and the higher-order modes [see Figs. 1(a) and 1(b)], inevitably leading to poor mode overlapping in X-cut TFLN. This poor overlap can be solved by adequately choosing a double-layered guiding structure of nonlinear and linear materials with similar refractive indices. As shown in Figs. 1(c) and 1(d), Luo *et al.* designed a TiO_2/LN semi-nonlinear nanophotonic waveguide with a significant overlap factor of 0.66[50].

In this study, as the orange region of the nonlinear response in Fig. 1(a) shows, the spatial asymmetry was destroyed when the nonlinear material (LN) was replaced with the linear material (TiO_2) in the semi-waveguide, which degraded the orange region of the nonlinear interaction to enhance optical overlapping. Compared with birefringent PM, this Type-0 (e + e → e) device with only a 2.35 mm length exhibits a considerable CE value of 650%/(W · cm^2), even when using the largest nonlinear

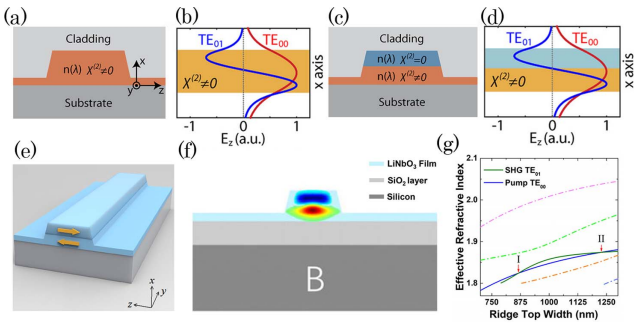

Fig. 1. (a)–(d) Symmetry of the ridge waveguide with diverse materials[50]. (a) Structure of monolithic nanophotonic waveguide. (b) High spatial asymmetry of two phase-matched modes around the *z*-axis component of the electric field. (c) Structure of a semi-nonlinear waveguide composed of two core materials. (d) Relative spatial symmetry of two phase-matching modes around the *z*-axis component of the electric field. (e)–(g) Scheme of the dual layers with reversed poling direction[45]. (e) Design of the geometrical parameters. (f) Double-layer TFLN waveguide with reverse polarization. (g) The relationship between the effective refractive index and etch depth.

coefficient and breaking the symmetric optical field profile. In addition, one novel technology based on the geometric dimension of the ridge waveguide in X-cut TFLN is shown in Figs. 1(e)–1(g), which not only exhibited a higher normalized conversion efficiency but also revealed the relationship between the effective refractive index and the etch depth (ranging from 750 nm to 1250 nm). Two TFLN layers with internally reversed poling direction were bonded to break the symmetry of the optical field profile between the two modes [see Fig. 1(e)], resulting in an ultrahigh conversion efficiency of 5540%/(W · cm^2) with intermodal PM[45]. In conclusion, both the birefringent PM and the intermodal PM hold excellent prospects in chip-scale nonlinear optics.

Although the conversion efficiency can be enhanced by nanowaveguides in birefringence PM or intermodal PM, these approaches are still in their infancy with the configuration of tightly light-confined. In addition, the higher-order wave mode shows a larger mode area, which can reduce the overlap coefficient of different modes. Hence, QPM is commonly performed in single-mode waveguides to obtain greater conversion efficiency (see Table 1). This QPM method shows that the ridge waveguides of PPLN thin film can provide a much higher conversion efficiency than the waveguides in the BPM or intermodal phase matching methods (see Table 1). With QPM, the energy flows continuously from the fundamental wave to the second-harmonic wave. Like other phase-matching methods, it also requires an intense light constraint to improve the conversion efficiency. The unique ability of the LN to reverse the domains periodically by applying an electric field forces the conversion efficiency to a higher level by compensating for the reciprocal lattice vector in the straight waveguide. In comparison to direct PM, as a tool for phase compensation, the QPM method shows more flexibility in operating wavelength, polarizations, and mode combinations by adjusting the poling period. Hence, a high-quality poling process should be one of the most distinctive methods.

Unlike other bulk reverse-proton-exchange (RPE) PPLN, the PPLN thin-film waveguide shows a higher strength of geometric dispersion, so its fabrication requires a shorter poling period (4–6 μm) for the telecom bands, which is more dependent on the fidelity of the poling technology. According to the literature, this technology in nanowaveguide construction was promising in effective on-chip nonlinear optics[21,57,58]. For example, Wang *et al.* fabricated a PPLN thin-film converter with high fidelity and a short, poled period (4 μm) in a duty cycle of ∼39% using the dry-etching method, which realized a high conversion efficiency of 2600%/(W · cm^2) with precise control of the poling uniformity[10]. However, this corrosive method with HF causes catastrophic damage to the waveguide so that it cannot be reused. Hence, it is necessary to improve the poling technology to achieve the repeatability of the poling process. To solve this problem, Fathpour *et al.* proposed an actively monitored ferroelectric domain reversal engineering method, including optically monitored iterative poling, depoling, and repoling, and produced a device with a normalized conversion efficiency of

4600%/(W · cm^2)[21], as shown in Figs. 2(a)–2(c). Furthermore, it was noted that this etch depth was 100 nm, which was smaller than the thickness of the thin film (300 nm) and which led to a smaller effective mode area and shorter poling period (2.67 μm) compared to the device with 300-nm-etch depth. This suggests that the shallow etched depth will significantly confine the electric field (e.g., the effective mode areas was 1.1 μm^2 in the telecom band, and 0.4 μm^2 in visible light band), which shows an effective nonlinear interaction with a small mode area [see Figs. 2(d)–2(f)][57]. Similarly, an ultrahigh conversion efficiency with 33000%/(W · cm^2) in a straight waveguide, as shown in Figs. 2(g)–2(i), was realized through strong light constraint and extremely short poling period (1.473 μm)[54]. However, this modulation band is in the deeper visible band (from the fundamental wave of 913 nm transfer to the second-harmonic wave of 456.5 nm) than the light at 775 nm, resulting in a smaller effective mode area and a more powerful nonlinear interaction. Meanwhile, this work shows the possibility of preventing perturbative light scattering by choosing the waveguide geometry with significant index contrast of the waves in fundamental and higher-order modes.

In conclusion, compared to birefringence phase matching and intermodal phase matching, QPM has become the mainstream phase-matching method in wavelength converters with high conversion efficiency. In order to achieve confined phase matching, the poling period needs to be decreased to 4–6 μm, (even 2 μm under special conditions) to adapt more substantial geometry dispersion, which creates the higher requirements for the poling process. Of course, there has been relevant research focusing on the optimization of the process, e.g., the actively monitored periodic poling[21,56].

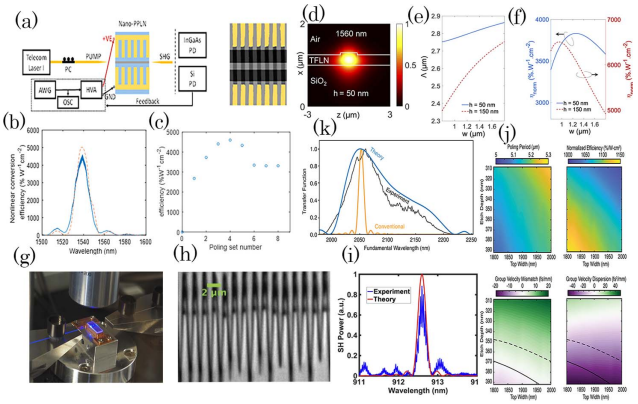

Fig. 2. (a)–(c) Experiment of the normalized conversion efficiency of 4600%/(W·cm^2)[21]. (a) Optimization of the poling process *in situ* using the iterative poling, depoling, and repoling sequence. (b) The relationship between the poling number and normalized conversion efficiency. (c) Measured peak conversion efficiency. (d)–(f) Experiment of the normalized conversion efficiency of the shallowly etched waveguide[57]. (d) Cross section of the shallowly etched waveguide at a depth of 50 nm in the X-cut waveguide. (e) Poling period. (f) Conversion efficiency of the structure. (g)–(i) Experiment of the normalized conversion efficiency of 33,000%/(W·cm^2)[40]. (g) Generation of the blue light in the PPLN thin film waveguide via SHG with ultra-high efficiency. (h) Poling period. (i) Normalized spectra of the blue second-harmonic generation. (j),(k) Ultrabroadband second-harmonic generation in the nano waveguide[54]. (j) Simulated poling period and normalized efficiency, respectively, as a function of the waveguide geometry. (k) Measured second-harmonic generation transfer function (black) for a 6-mm-long nanophotonic waveguide, showing a good agreement with the theory (blue).

2.1.2. Wide bandwidth

In addition to the conversion efficiency, the bandwidth is another crucial aspect of concern that needs to be evaluated for the tunability of the frequency of the wavelength converters. A broader bandwidth drives the more extensive applications of the laser with high power. As shown in Table 1, the full-width at half-maximum (FWHM) of the wavelength converters with ultra-high conversion efficiency is lower than 20 nm because of the material dispersion[53,54,56,57,59,60]. In compensating for the material dispersion, the step-chirped PPLN thin-film waveguide was fabricated to support different wavelengths. With the fluctuation of the wavelength, the effective refractive index of the material changed, which makes the poling period different in a straight waveguide. Hence, Bo *et al.* fabricated the PPLN thin-film waveguide with the step poling period ranging from $\Lambda_1 = 4.064\,\mu m$ to $\Lambda_{49} = 4.110\,\mu m$[61]. The step poling period introduced the rich reciprocal vectors match that led to the tunability of the wavelength. However, it is worth noting that the second harmonic was generated from 1550 nm to 1660 nm (110 nm) of the pump despite the cost of a low conversion efficiency of 9.6%/(W · cm^2). In addition to the step-chirped waveguide, a high wavelength tunability could also be achieved by regulating the refractive index at different temperatures[49]. This capability of temperature sensitivity promotes the high tunability in the PM of the wavelength with a tuning slope of 0.84 nm/K at the cost of a low conversion efficiency under 22.2%/(W · cm^2).

However, the problem of balancing the wide bandwidth and the conversion efficiency still needs to be solved[62]. For example, the most effective way to avoid a narrow bandwidth is to reduce the length of the waveguide to that much smaller than coherent length, but this can severely limit the conversion efficiency. Hence, to solve these two potential defect issues, one of the approaches is to simultaneously satisfy the group velocity match and the group velocity dispersion with the pump of the pulse, which can result in the nonlinear relationship between the bandwidth and the device length [see Fig. 2(j)]. Jankowski observed this phenomenon in a PPLN thin-film nanowaveguide, which indicated that a conversion efficiency of 1000%/(W · cm^2) was achieved with a bandwidth broader than 110 nm [see Fig. 2(k)] by adjusting the group velocity match and the group velocity dispersion in a pulse pump power (wavelength of pump is about 2 μm) lower than 100 fJ[54].

Overall, the tunable wavelength can be realized using the thermal birefringence effect of the LN, which is promising for the efficient tunable visible light source. In addition, a bandwidth more than 100 nm could be achieved by selecting a domain structure or optimizing dispersion engineering. However, wide bandwidth performance based on dispersion optimization is

primarily produced in the pulse pump. Therefore, the bandwidth will be greatly limited if using the dispersion engineering method with a continuous wave pump.

2.2. Other nonlinear effects in wave optics

In addition to SHG, many types of research focusing on wavelength conversion have also been accomplished through SFG and DFG based on second-order nonlinear processes.

2.2.1. Sum frequency generation

Compared with SHG, SFG is more promising for mixed fields of two distinctive wavelengths and can broaden the spectral ranges the SHG cannot reach. Moreover, people found that the far-infrared and sub-THz waves can be converted to visible light through the process of SFG to solve the scarcity of detectors of the far-infrared and sub-THz waves[63,64]. Rao *et al.* proposed the SFG bandwidth of ~20 nm with a conversion efficiency of $900\%/(\mathrm{W}\cdot\mathrm{cm}^2)$[21]. In addition, Chen *et al.* proposed a PPLN thin film with a bandwidth of 15 nm by significantly satisfying the QPM and decreasing the group velocity mismatching (GVM) simultaneously under a low conversion efficiency of 3.3%/W due to the modulation of the fifth-order instead of the first-order[65]. Although the performance of a single SFG process is less well developed than the SHG process, it also plays an essential role in cascading nonlinear effects, which can enrich the applications of nonlinear optics.

What makes the cascaded effects is that the SHG effect commonly accompanies the SFG to mimic the third-order nonlinear effect, which can broadcast the wavelength. However, compared with a single SFG process in the straight waveguide, these cascaded second-order nonlinear processes were mainly realized in resonators[66-69]. As an example, a resonator with a high Q-factor of 3×10^6 and with cascaded nonlinearity [SHG, SFG, and stimulated Raman scattering (SRS)] was fabricated, which emitted green light and blue light by tuning the pump power[70]. With the increase of the pump power, colorful nonlinear effects were observed, which generated more applications in integrated nonlinear optics[71]. In addition, these cascaded nonlinear processes would reach a lower input power (~mW), which would be more stable with the reduction of the thermal and photorefraction effects compared with a pure third-order nonlinear process[72,73].

Presently, the technology of devices based on the SFG effect is less well established than those based on the SHG effect, but it fills the absent band range of the SHG effect to adapt to the increasing data rate of optical communication. Especially in resonators, the intermodal PM was used to efficiently produce cascaded processes, introducing a third-harmonic generation (THG) effect by cascading the χ^2-based process instead of the single χ^3-based process. As a promising candidate for nonlinear devices with the freedom to choose operation wavelengths, the resonator could achieve more excellent characteristics by increasing the quality factor[74–77].

2.2.2. Difference frequency generation

For enriching the nonlinear processes in the nonlinear process, another wavelength conversion of the DFG effect was investigated. As mentioned above, most devices do not generate mid-infrared light due to the absence of a needed light source, which cannot meet the demand of optical communication, environmental monitoring, and spectroscopy research. This process is also a nonlinear interaction of three waves like SFG. However, unlike the SFG process, this process exhibits a frequency-down conversion instead of a frequency-up conversion. The mid-infrared light around 3660 nm via the DFG effect was produced in a thin-film LN waveguide with a sapphire substrate[78]. The field can be tightly confined to reach a high efficiency of $200\%/(\mathrm{W}\cdot\mathrm{cm}^2)$ because of the lower absorption loss in the sapphire substrate instead of the silica substrate[78]. With a higher conversion efficiency in the pure DFG process, Zhu *et al.* performed an active domain structure monitoring method to fabricate a PPLN thin film with a ultra-high efficiency of $10,300\%/(\mathrm{W}\cdot\mathrm{cm}^2)$, making the spectral tuning range of the generated idler in the C-band about 50 nm[56]. In telecommunications, the DFG could be achieved with a higher conversion efficiency than the mid-IR band. Hence, although the sapphire substrate realized a lower absorption loss in the mid-IR band, there still is a long way to go for producing mid-IR light effectively.

3. Optical Parametric Amplifier Based on TFLN

With respect to inline optical repeaters, optical amplifiers can compensate for signal transmission loss to achieve long-distance transmission in a WDM transmission system. Hence, as a promising device, the optical parametric amplifier (OPA) attracts significant attention for delivering a flat gain spectrum with low noise figure in optical communications. The optical amplifier amplifies the input optical power, which is widely used in optical communications[79–81], optical imaging[82,83], optical networking[84,85], computing[86,87], and quantum information processing[88,89], especially in telecom communications.

OPA is mainly based on the DFG process and is composed of signal gain, noise figure, and bandwidth parameters. There are many types of optical amplifiers, including semiconductor optical amplifiers (SOAs)[90], χ^3-based optical amplifiers[91], rare-earth-doped optical amplifiers[92–94], and χ^2-based optical amplifiers[97,98]. Here, we mainly compare the properties of different optical amplifiers, such as gain, bandwidth, and noise figures based on thin-film LN (see Table 2). Unlike the optical converter, the performance of the OPA can be expressed by signal light instead of idler light, such as $\mathrm{Gain}=10\log_{10}(\frac{P_{\mathrm{signal,out}}}{P_{\mathrm{signal,in}}})$. The unique bandwidth was also crucial due to its degree of wavelength dependence. Moreover, the amplifier's noise figure (NF) was described to explain the production of specific noise in the amplification process, which will limit the transmission process of a communication system.

Table 2. Comparison of Different Amplifiers Based on TFLN.

Type	Length (mm)	Gain (dB)	Pump (W)	Signal Wavelength (nm)	Bandwidth (nm)	NF (dB)	Year	Ref.
cSHG/DFG	20	38.3	12.589	1550	~100	–	2018	[95]
cSHG/DFG	50	18.6	1.38	1538	61.6	–	2016	[96]
DFG*	45	24.7	1.3	1553.3	68	4	2021	[97]
DFG※	45	30	1.3	1553.3	68	1	2021	[97]
DFG	6	30	0.3	2090	–	–	2022	[98]

Note: The type with * and ※ represents phase-insensitive amplification (PIA) and phase-sensitive amplification (PSA).

Many researchers have explored rare-earth-doped TFLN and recently made breakthroughs[92,93,99,100]. However, this type of optical amplification is fabricated by the excitation of ions instead of the nonlinear effect on the etched waveguide, so it remains a challenge with regard to ion absorption loss[93] and noise caused by extra amplified spontaneous emission (ASE), which are difficult to eliminate.

Another necessary amplifier discussed in this review is based on the nonlinear effect of an OPA. The inherent characteristic of the OPA is that when the signal light is amplified, idler light is generated at a wavelength symmetric to the center of the OPA band[101]. As shown in Table 2, the length of the commercialized PPLN modules (from 20 mm to 50 mm) is commonly larger than that of the experimentally fabricated waveguides (6 mm) used for the OPA. This design includes cascaded SHG and DFG effects in one module, which can improve the gain and increase the bandwidth. In a single module, the OPA was designed based on bulk PPLN with a low net gain of 18.6 dB due to lower pump power[96]. Hence, the pump power could be larger for higher gain. As shown in Table 2, a significant gain (38.3 dB) can be achieved over a wide bandwidth (tens of nm) because the poling periods (about 17 μm) required by these two effects (SHG and DFG) are roughly the same[95]. However, since this high gain should be achieved with the input of a high pump power over 12.589 W, which would influence the temperature of the chip, the stability of the chip will be affected greatly. In multiple modules, as shown in Figs. 3(a)–3(c), the high noise figure was reduced, and the crosstalk was induced, by the optical parametric interaction between the DWDM channels, which was mitigated by using 2-stage configuration cascading of two PPLNs for the SHG and the OPA[97]. This amplification should be phase-sensitive. It can reach a high gain of 30 dB with a noise figure lower than 1 dB, which is promising for achieving a higher signal-to-noise ratio in future high-capacity optical communications[97]. Also, extra gain (~6 dB) and noise reduction can be achieved in optical parametric amplification by introducing idler light that is conjugated to the signal light. Although the system highly improves the noise of the optical amplifiers, it also challenges the integration of the optical amplifiers. Hence, the TFLN shows great prospects in the OPA with high-density light. As shown in Table 2, the high gain of 30 dB [see Fig. 3(e)] has been achieved in a 6-mm-PPLN thin-film nanowaveguide injected by a pump power of only 0.3 W, which was lower than that of the bulk PPLN waveguide.

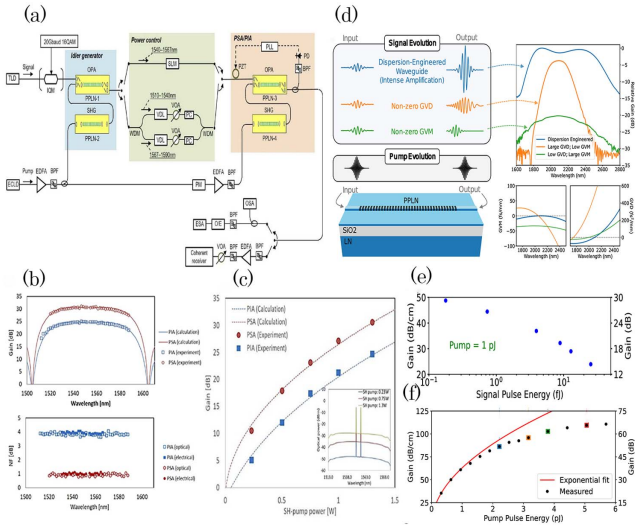

Fig. 3. (a)–(c) PPLN-based non-degenerate phase-sensitive amplifier[97]. (a) Experimental setup for the PSA. (b) Bandwidth and NF of the cascaded SHG/OPA amplifier. (c) The relationship between the gain and the SH-pump power. PSA, phase sensitive amplification; PIA, phase insensitive amplification. (d)–(f) The degenerate OPA based on the nanowaveguide[98]. (d) Waveguides engineering for the GVD and the GVM in maximizing the OPA performance. (e) Measured saturated gain versus the input signal pulse. (f) Extracted gain versus the pump pulse energy.

Leveraging a flexible design of dispersion engineering, the bandwidth of the OPA is superior to other amplification[90,102–105]. As shown in Fig. 3(d), this OPA is based on PPLN thin film and can provide a flexible geometry design, which simultaneously leads to a wide bandwidth and high gain[98]. The feasible geometry waveguide was designed to satisfy the dispersion engineering, including group velocity mismatching (GVM) and group velocity dispersion (GVD), which means the amplification bandwidth of the OPA depends on the phase-matching characteristics in a nonlinear optical medium. It was noted that this process was the degenerate optical

parametric amplification with a gain of 30 dB and a pump power of 0.3 W [as shown in Figs. 3(a) and 3(b)]. However, this amplification would reach a saturated state, as shown in Fig. 3(e). Hence, the amplifier in the optical parametric generation (OPG) was operated to avoid the saturation effect that led to a parametric generation of 66 dB [see Fig. 3(f)] and an ultra-wide bandwidth of 380 nm, which was much broader than in other mechanisms[98]. The length of the nanowaveguide (6 mm) is much shorter than the commercialized length, which is more conducive for integrating compact devices[106]. These studies showed that the intensity of the manufacturing errors could be eliminated through dispersion engineering. However, the noise of the amplification process still needs further study. We look forward to its rapid development on the road to commercialization.

In conclusion, since the thickness of the commercialized OPA is on the micron scale, it is impossible for it to be conducive to integrated optics. However, the noise figure of these commercialized devices can be greatly reduced by cascaded processes and other operations. Compared with the waveguide with thickness of 4–5 μm core layer, the noise figure improvement would be a hot topic for nanowaveguides. Although improving the NF in the nanowaveguides is still in its infancy, the on-chip waveguide shows excellent performances in gain and bandwidth. When the OPA is in vacuum fluctuations, this TFLN-based device achieves high gain and wide bandwidth using dispersion engineering, which shows superb potential in optical amplification.

4. Optical Parametric Oscillator

Optical parametric oscillation (OPO) is an essential source of internal radiation in infrared spectroscopy fields and has excellent development areas from multi-channel optical communications to lidar[107]. It is a nonlinear optical frequency conversion process that converts light with a short wavelength (pump) to parametric light with longer wavelength (signal and idler wave). Its development trend mainly includes a low threshold value of the pump, a widely-tunable range of wavelength, miniaturization, a high output power (high conversion efficiency), and substantial stability. Unlike the DFG effect, which needs the input signal in advance, the OPO only needs inject the pump light, which saves the light source. Meanwhile, the parametric light becomes oscillated and highly constrained due to the introduction of the PPLN thin film-based resonant cavity. Hence, the equivalent intensity of oscillation in the cavity can be increased hundreds of times, which greatly reduces the threshold power (~microwatt) as compared with crystal OPO (~milliwatt and watt)[108–112]. In order to reduce the threshold in the resonators, the standard method is to improve the Q-factor when the optical loss and the optical gain are balanced. For example, Cheng *et al.* proposed an on-chip microdisk resonator with a Q-factor above 10^8 with only a 19.6 mW threshold [see Figs. 4(a) and 4(b)][113]. Although the bulk whispering gallery resonator (WGR) may realize a higher Q-factor above 10^9, the thin-film microdisk

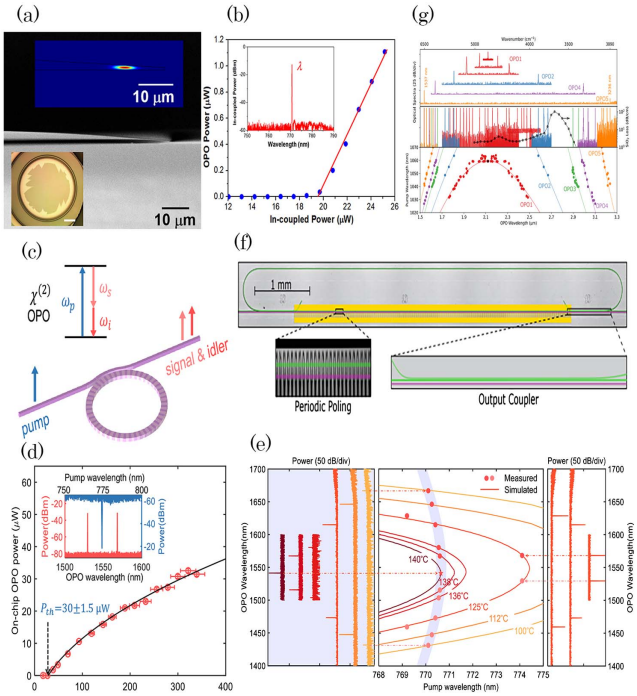

Fig. 4. (a),(b) Microdisk of the high Q-factor[113]. (a) The zoom-in SEM image of the sidewall from the side view. Upper inset: the electric field distribution; lower inset: the optical micrograph of the resonator, showing a relatively small pillar whose rough boundary is far from the periphery of the resonator, where the scale bar is 200 μm. (b) Power dependence of the OPO, showing a threshold pump power of ~19.6 μW and a gain rate of 20%. (c)–(e) Periodically poled lithium niobate microring resonator (PPLNMR) with a low threshold in temperature tunability[58]. (c) Illustration of the parametric oscillation using PPLNMR. (d) The experimental (red circles) and theoretical (solid line) on-chip infrared power versus the on-chip pump power for the parametric oscillation process. An example of the snapshot of the off-chip pump (blue) and parametric oscillation (red) spectra after the device as shown in the inset. (e) The OPO wavelength tuning by varying both the temperature and pump wavelength. Middle panel: simulated (solid lines) and measured (circles) OPO wavelengths versus the pump wavelength at various temperatures. As an example, the right panel plots the recorded spectra with different pump wavelengths at 125°C. The left panel indicates the occurrence of degenerate parametric oscillation by varying the temperature. (f),(g) The OPO with the racetrack[107]. (f) Design of the OPO with the racetrack. (g) Wavelength tuning range.

(~600 nm) showed possibilities of on chip-scale miniaturization ~2 orders of magnitude thinner than the bulk crystals. Hence, Tang *et al.* described a PPLN resonator with a relatively low threshold of 30 mW with a lower Q-factor of 0.6×10^6 compared with the bulk WGR[11], which presents potential in the threshold of picowatts with the Q-factor approaching 10^8. In conclusion, the whisper gallery mode (WGM) with a high Q can confine the light in small mode volume for a long time, which can enhance the nonlinearity[114–116].

However, despite significant progress in the ultralow threshold, it is noted that the OPO shows a low threshold at the expense of limited wavelength tunability[117]. The wide tunability with mid-infrared coverage still needs to be improved in

optical communications. Hence, future investigations are demanding to extend the optical tunable band from the near-infrared to the mid-infrared band. In Section 2.2.2, as we mentioned before, mid-infrared light was generated by the DFG process. Similarly, the mid-infrared light could also be generated by a widely-tunable OPO. Due to the dispersion of the material, the OPO can control the parametric wavelength over a broad range by tuning the temperature from 100°C to 140°C. As shown in Fig. 4(e), the OPO wavelength based on the PPLN thin film [see Figs. 4(c) and 4(d)] could be tuned from 1460 nm to 1630 nm[58]. Although it showed reasonable control over a relatively wide bandwidth range, it showed limitations in the tunability of the mid-infrared wavelength. Hence, another method (proposed in Section 2.1.2) was used to broaden the bandwidth by fabricating the OPO with step poling periods[107] in the PPLN thin-film racetrack. As shown in Figs. 4(f) and 4(g), this device was designed with a doubly resonant chip-scale, which can be widely tunable from 1530 nm to 3250 nm (over 1.7 μm)[107]. This racetrack has extensively promoted the development of tunable light sources from multi-channel optical communications to lidar.

Overall, OPO is moving towards a low threshold, compact structure with high conversion efficiency and wide tunability. By incorporating quadratic nonlinearity into the OPO and improving the *Q*-factor of the on-chip device, a stronger interaction could be achieved at a lower pump power, and other nonlinear competitive processes could be reduced. Of course, in order to tune the OPO not only in the near-infrared band but also in the mid-infrared band, some characteristics should be implemented to expand the tunable range of the wavelengths, but this could increase the threshold.

5. Optical Frequency Comb Based on Nonlinear-Wave Interaction

An optical frequency comb (OFC) is a steady pulse-sequence beam in the time domain and a suite of equidistant spectral lines in the frequency domain. At present, the OFC is the most effective tool for absolute optical frequency measurements, providing an ideal research tool for precision spectroscopy, chemical sensing, timekeeping, quantum manipulation, and being a source of wavelength division multiplexing in optical communications. The prevailing method for generating OFC is commonly based on the Kerr effect. Much research regarding OFC has been reported and shown great progress[118–122] (details can be seen in Ref. [123]). This section mainly deals with all-optic quadratic nonlinear effects, so the electro-optic OFC will not be introduced here.

As we all know, the technology of the all-optic nonlinear OFC based on the LN platform also developed rapidly. Although people usually use the third-order nonlinear characteristics of LN to produce the Kerr effect to then realize the OFC[124–126], the intrinsically higher strength of the second-order nonlinear property was effectively investigated for its higher tolerance of power density and its *Q*-factor. It has been reported that the OFC can

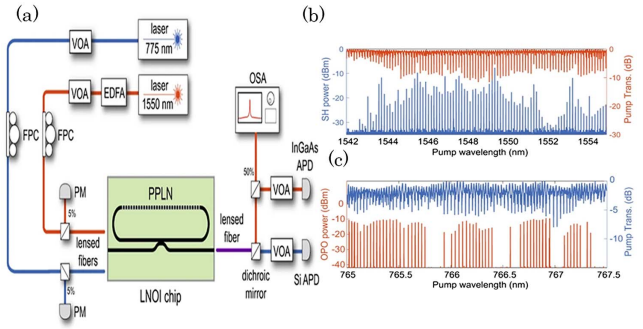

Fig. 5. (a)–(c) OPO resonant device[117]. (a) Resonant second-order nonlinear optical device. (b) Scanning the near-infrared laser shows that second-harmonic generation occurs at wavelengths corresponding to the modes of the resonator. (c) Scanning the blue pump laser across the wavelength shows that many resonances surpass the parametric oscillation threshold.

be directly realized in LN by a pure second-order nonlinear process. However, recent studies indicate the OFCs can also be realized by OPO cascading other second-order nonlinear effects (such as SHG, SFG, and DFG), which could generate widely spanning comb spectra[110,117]. When the pump power (280 mW) exceeds the threshold power, an OFC with a bandwidth of 60 nm was generated in a straight waveguide of a PPLN thin film through the SHG-OPO processes[127]. In addition, the OPO is formed by a reflective coating at both ends of the waveguide, causing a limited spectral range. However, as expected, the properties of the above crystal device were not the same as those with the low threshold and high tunability. Therefore, to reduce the threshold and increase the tunability simultaneously, the photonic circuit based on the TFLN was proposed, as shown in Figs. 5(a)–5(c), which achieved a more than 1 THz bandwidth with a threshold of tens of micro-watts through optical oscillation[117]. To further extend the wavelength tuning range, the PM was satisfied by controlling the temperature, which showed a wider range of tunable wavelengths [from 1400 nm to 1700 nm at the temperature of 125°C, see Fig. 4(e)][11].

Unlike third-order nonlinear effects, these materials with quadratic nonlinearity allow more feasibility in the arrangement of the comb spectra by controlling the PM through poling technology. In addition, the oscillation threshold can be significantly reduced in microring resonators based on PPLN thin film, and the wavelength tunability can be increased by adjusting the operating temperature. However, the control of the temperature puts a higher requirement on the fabrication process, such as the different coefficients of thermal expansion of the LN, which can limit the compatibility with other fabrication steps. Of course, higher performance can also be achieved by more stringent conditions on phase matching and group velocity mismatch[42].

6. All-Optical Switch Based on Nonlinear Optics

As the critical device for switching optical paths, the optical switch plays a vital role in dense wavelength division

multiplexing (DWDM), improvement of the optical transmission rate, and optical computing platform. Meanwhile, the optical switch is one of the core components of an optical beamforming network in wideband array electronic information systems[128]. At present, the material refractive index of most optical switches based on TFLN can be adjusted in the temperature and electric field, leading to the control of the on-and-off state of the device. Guo *et al.* proposed the all-optical switch, which was composed of a PPLN thin-film waveguide and an adjacent directional coupler[34]. Two distinct phase-matching [SHG and degenerate optical amplifier (DOPA)] engineering mechanisms were cascaded by the poling defect in a straight waveguide. This device showed a good performance over ultralow switching energies down to 80 fJ and a fastest switching time of ~46 fs (≪ 1 ns). Compared with other optical switches based on third-order harmonic generation in the cavity, this waveguide of the nanostructure in the QPM method reduced the switching time by introducing large second-order nonlinearity of LN.

7. Conclusions, Challenges, and Perspectives

Because of the revolutionary progress in TFLN technology and engineering technologies, LN has received much attention in integrated nonlinear optics. In particular, the TFLN retained bulk inherent characteristics of higher strength of the quadratic nonlinear effect than cubic nonlinear effects, which were easy to integrate and which led to versatile applications in the χ^2-based all-optical nonlinear field. This nonlinear optics chip could create and operate signals with surpassed metrics over possible electronically especially for the transmission speed of light[129]. In this review, we have discussed the recent progress of TFLN and the key performance of the nonlinear all-optical devices, including wavelength converters, optical amplifiers, optical frequency combs, optical parametric oscillators, and optical switch.

First, we briefly described the excellent feature of the TFLN material in integrated optics. Next, we discussed the full investigation of the multiple nonlinear devices with a great deal of high performances, informing the nanostructure of the waveguide has highly outperformed the structure of bulk and thin-film LN in light constraints, power consumption, and bandwidth. In addition, the waveguide coupling with fiber, which could capture more light into the device as compared with the structure of metasurface, led to a great prospect for photonic integrated circuits (PICs). Hence, further research needs to be done in reducing the transmission and fiber-to-chip coupling losses in the TFLN waveguide[130]. However, unlike the electro-optic effect in the TFLN waveguide, the all-optical χ^2-based nonlinear effect can be achieved by compensating the phase mismatching of the field instead of implementing the voltage, especially for the PPLN thin-film ridge waveguides, whose potential is not only the manufacturing progress but also the design's flexibility. As a flexible toolbox for phase matching, much smaller poling periods are involved in PPLN thin film routes making thin-film LN more competitive and unique in comparison with other nonlinear materials in integrated nonlinear optical platforms. Hence, PPLN thin film has generated a new collection of influential integrated χ^2-based optical devices, which is evident by orders of magnitude higher efficiencies of wavelength converters based on PPLN thin film than bulk RPE PPLN waveguides[10]. In addition, the optical parametric amplifier, the optical parametric oscillator, the optical frequency comb, and the optical switch with inspirational properties have been verified on the LN platform.

Despite of the TFLN-based devices' remarkable revolution in versatile applications, these applications still suffer from some challenges in several areas. First of all, with respect to a single device to elaborate, further optimization of the materials will be urgently prepared to reach a device with cheap, high quality, and outstanding performance. This optimization includes the design of the device's geometry (e.g., precise dispersion engineering and phase matching), the fabrication of a high-fidelity device (etching, poling, doping, and annealing)[34], and the universality of the experimental environment (e.g., the fluctuation of temperature and the utilization of the pump's type). Although nonlinear optical effects have been experimentally demonstrated in TFLN nanostructured waveguides, continuous laser pumping, which only requires a semiconductor laser, was preferentially needed when compared with pulsed pumping, which has a high cost due to material loss. This limited use of a continuous laser pump is particularly evident in the net gain of the continuous wave amplification of signals[91,131] which is less capable for telecommunication operation. A potential solution to this problem is to reduce the loss of the TFLN waveguide. Thus, lower loss is still expected to realize a mass-produced, low-cost, and high-quality device in spite of achieving an ultra-low loss (0.027 dB/cm[132]) in the LN platform. However, reducing single-mode propagation loss to 0.01 dB/cm is still a great challenge. Thus, further studies of technology with surface fabrication and polishing are in demand. For example, scattering loss is inevitably produced due to the roughness of both sides of the etched ridge waveguide, which brings higher requirements for technology and equipment. Another approach is to fabricate the device with a shallow-etched waveguide (with an etched depth of less than 200 nm). Meanwhile, one should be aware of the extra lateral leakage loss when designing the morphological parameters of the waveguide[133,134].

In addition, in terms of specific functional devices, the efficiency and bandwidth could be improved by carefully tuning the degree of light-coupling, dispersion engineering, and fabrication technology (e.g., high-quality factor). From an applications standpoint, more powerful overlap coefficients are more adoptable as compared with high-fidelity fabrication due to the high tolerance of the fabrication defect[135]. In the optical parametric amplification process, the optical parameters will not completely degenerate after participating in the interaction, so, if it is the second-harmonic inverse process, there will be errors in the measurement of the gain and bandwidth. Because the bands of signal light and idler light are close to each other, the idler light cannot be accurately filtered by the filter,

so rarely do studies in the research indicate that the signal light and idler light can be separated. In addition, it was noted that high-quality χ^2-cascaded processes will drive the generation of efficient OFCs in order to promote their capacity to achieve minimization and commercialization. These all-optical devices based on TFLN can greatly improve the speed of information processing. This fast-response was evident in the optical switch, which realized femtosecond switch times instead of picosecond switch times.

As the perspective for the all-optical nonlinear devices, the appearance of TFLN provides more creative possibilities for all-optical communication on chip-scale circuits, which are more conducive to high-speed data transmission. In addition, because of its design, fabrication, and integration, versatile applications push the TFLN-based platform to break through the challenges. It is believed that the TFLN platform will continue to develop rapidly, and the high yield of the devices will be realized in the near future, which will provide many new opportunities in the related fields.

Acknowledgement

This work was supported by the National Key R&D Program of China (No. 2021YFB2800700), the National Natural Science Foundation of China (Nos. 62275047, 61875241, and 22102023), the Fellowship of China Postdoctoral Science Foundation (Nos. 2021M700768 and 2022M710672), and the Natural Science Foundation of Jiangsu Province (No. BK20220816).

†These authors contributed equally to this work.

References

1. R. Wu, L. Gao, Y. Liang, Y. Zheng, J. Zhou, H. Qi, D. Yin, M. Wang, Z. Fang, and Y. Cheng, "High-production-rate fabrication of low-loss lithium niobate electro-optic modulators using photolithography assisted chemo-mechanical etching (PLACE)," Micromachines **13**, 378 (2022).
2. T. Gaur, P. Mishra, G. Hegde, and T. Srinivas, "Modeling and analysis of device orientation, analog and digital performance of electrode design for high speed electro-optic modulator," Photonics **10**, 301 (2023).
3. S. Zhu, Y. Zhang, Y. Ren, Y. Wang, K. Zhai, H. Feng, Y. Jin, Z. Lin, J. Feng, S. Li, Q. Yang, N. H. Zhu, E. Y.-B. Pun, and C. Wang, "Waveguide-integrated two-dimensional material photodetectors in thin-film lithium niobate," arXiv:2212.01991 (2022).
4. S. Dutta, Y. Zhao, U. Saha, D. Farfurnik, E. A. Goldschmidt, and E. Waks, "An atomic frequency comb memory in rare-earth-doped thin-film lithium niobate," ACS Photonics **10**, 1104 (2023).
5. F. I. Baida, J. J. Robayo Yepes, and A. Ndao, "Giant second harmonic generation in etch-less lithium niobate thin film," J. Appl. Phys. **133**, 124501 (2023).
6. G. H. Y. Li, R. Sekine, R. Nehra, R. M. Gray, L. Ledezma, Q. Guo, and A. Marandi, "All-optical ultrafast ReLU function for energy-efficient nanophotonic deep learning," Nanophotonics **12**, 847 (2023).
7. J. Ling, J. Staffa, H. Wang, B. Shen, L. Chang, U. A. Javid, L. Wu, Z. Yuan, R. Lopez-Rios, M. Li, Y. He, B. Li, J. E. Bowers, K. J. Vahala, and Q. Lin, "Self-injection locked frequency conversion laser," Laser Photonics Rev. **17**, 2200663 (2023).
8. J. Mishra, T. P. McKenna, E. Ng, H. S. Stokowski, M. Jankowski, C. Langrock, D. Heydari, H. Mabuchi, M. M. Fejer, and A. H. Safavi-Naeini, "Mid-infrared nonlinear optics in thin-film lithium niobate on sapphire," Optica **8**, 921 (2021).
9. B. S. Elkus, K. Abdelsalam, S. Fathpour, P. Kumar, and G. S. Kanter, "Quantum-correlated photon-pair generation via cascaded nonlinearity in an ultra-compact lithium-niobate nano-waveguide," Opt. Express **28**, 39963 (2020).
10. C. Wang, C. Langrock, A. Marandi, M. Jankowski, M. Zhang, B. Desiatov, M. M. Fejer, and M. Lončar, "Ultrahigh-efficiency wavelength conversion in nanophotonic periodically poled lithium niobate waveguides," Optica **5**, 1438 (2018).
11. J. Lu, A. Al Sayem, Z. Gong, J. B. Surya, C.-L. Zou, and H. X. Tang, "Ultralow-threshold thin-film lithium niobate optical parametric oscillator," Optica **8**, 539 (2021).
12. J. Hamazaki, Y. Ogawa, T. Kishimoto, S. Hayashi, N. Sekine, and I. Hosako, "Conversion efficiency improvement of terahertz wave generation laterally emitted by a ridge-type periodically poled lithium niobate," Opt. Express **30**, 11472 (2022).
13. I. Shoji, T. Kondo, A. Kitamoto, M. Shirane, and R. Ito, "Absolute scale of second-order nonlinear-optical coefficients," J. Opt. Soc. Am. B **14**, 2268 (1997).
14. W. H. P. Pernice, C. Xiong, C. Schuck, and H. X. Tang, "Second harmonic generation in phase matched aluminum nitride waveguides and micro-ring resonators," Appl. Phys. Lett. **100**, 223501 (2012).
15. J. Lin, F. Bo, Y. Cheng, and J. Xu, "Advances in on-chip photonic devices based on lithium niobate on insulator," Photonics Res. **8**, 1910 (2020).
16. M. De Micheli, J. Botineau, P. Sibillot, D. B. Ostrowsky, and M. Papuchon, "Fabrication and characterization of titanium indiffused proton exchanged (TIPE) waveguides in lithium niobate," Opt. Commun. **42**, 101 (1982).
17. M. De Micheli, J. Botineau, S. Neveu, P. Sibillot, D. B. Ostrowsky, and M. Papuchon, "Independent control of index and profiles in proton-exchanged lithium niobate guides," Opt. Lett. **8**, 114 (1983).
18. P. M. Read, S. P. Speakman, M. D. Hudson, and L. Considine, "An ion beam investigation of the preliminary stages of titanium indiffusion in lithium niobate waveguides," Nucl. Instrum. Methods Phys. Res. Sect. B Beam Interact. Mater. At. **15**, 398 (1986).
19. I. E. Barry, G. W. Ross, P. G. R. Smith, and R. W. Eason, "Ridge waveguides in lithium niobate fabricated by differential etching following spatially selective domain inversion," Appl. Phys. Lett. **74**, 1487 (1999).
20. R. V. Schmidt and I. P. Kaminow, "Metal-diffused optical waveguides in $LiNbO_3$," Appl. Phys. Lett. **25**, 458 (1974).
21. A. Rao, K. Abdelsalam, T. Sjaardema, A. Honardoost, G. F. Camacho-Gonzalez, and S. Fathpour, "Actively monitored periodic-poling in thin-film lithium niobate photonic waveguides with ultrahigh nonlinear conversion efficiency of 4600% W^{-1} cm^{-2}," Opt. Express **27**, 25920 (2019).
22. J. Sun and C.-Q. Xu, "Green-induced infrared absorption in annealed proton-exchanged MgO:$LiNbO_3$ waveguides," J. Opt. Soc. Am. B **31**, 2779 (2014).
23. M. Levy, R. M. Osgood, Jr., R. Liu, L. E. Cross, G. S. Cargill, III, A. Kumar, and H. Bakhru, "Fabrication of single-crystal lithium niobate films by crystal ion slicing," Appl. Phys. Lett. **73**, 2293 (1998).
24. Y. Jia, L. Wang, and F. Chen, "Ion-cut lithium niobate on insulator technology: recent advances and perspectives," Appl. Phys. Rev. **8**, 011307 (2021).
25. G. Poberaj, H. Hu, W. Sohler, and P. Günter, "Lithium niobate on insulator (LNOI) for micro-photonic devices," Laser Photonics Rev. **6**, 488 (2012).
26. A. Honardoost, K. Abdelsalam, and S. Fathpour, "Rejuvenating a versatile photonic material: thin-film lithium niobate," Laser Photonics Rev. **14**, 2000088 (2020).
27. A. Boes, B. Corcoran, L. Chang, J. Bowers, and A. Mitchell, "Status and potential of lithium niobate on insulator (LNOI) for photonic integrated circuits," Laser Photonics Rev. **12**, 1700256 (2018).
28. https://www.nanoln.com/.
29. J. Zhao, C. Ma, M. Rüsing, and S. Mookherjea, "High quality entangled photon pair generation in periodically poled thin-film lithium niobate waveguides," Phys. Rev. Lett. **124**, 163603 (2020).
30. J. Yang and C. Wang, "Efficient terahertz generation scheme in a thin-film lithium niobate-silicon hybrid platform," Opt. Express **29**, 16477 (2021).
31. H. T. Olgun, W. Tian, G. Cirmi, K. Ravi, C. Rentschler, H. Çankaya, M. Pergament, M. Hemmer, Y. Hua, D. N. Schimpf, N. H. Matlis, and F. X. Kärtner, "Highly efficient generation of narrowband terahertz radiation driven by a two-spectral-line laser in PPLN," Opt. Lett. **47**, 2374 (2022).

32. Q. Guo, R. Sekine, L. Ledezma, R. Nehra, D. J. Dean, A. Roy, R. M. Gray, S. Jahani, and A. Marandi, "Femtojoule femtosecond all-optical switching in lithium niobate nanophotonics," Nat. Photonics **16**, 625 (2022).
33. P. Minzioni, C. Lacava, T. Tanabe, J. Dong, X. Hu, G. Csaba, W. Porod, G. Singh, A. E. Willner, A. Almaiman, V. Torres-Company, J. Schröder, A. C. Peacock, M. J. Strain, F. Parmigiani, G. Contestabile, D. Marpaung, Z. Liu, J. E. Bowers, L. Chang, S. Fabbri, M. R. Vázquez, V. Bharadwaj, S. M. Eaton, P. Lodahl, X. Zhang, B. J. Eggleton, W. J. Munro, K. Nemoto, O. Morin, J. Laurat, and J. Nunn, "Roadmap on all-optical processing," J. Opt. **21**, 063001 (2019).
34. D. Zhu, L. Shao, M. Yu, R. Cheng, B. Desiatov, C. J. Xin, Y. Hu, J. Holzgrafe, S. Ghosh, A. Shams-Ansari, E. Puma, N. Sinclair, C. Reimer, M. Zhang, and M. Lončar, "Integrated photonics on thin-film lithium niobate," Adv. Opt. Photonics **13**, 242 (2021).
35. G. Chen, N. Li, J. D. Ng, H.-L. Lin, Y. Zhou, Y. H. Fu, L. Y. T. Lee, Y. Yu, A.-Q. Liu, and A. J. Danner, "Advances in lithium niobate photonics: development status and perspectives," Adv. Photonics **4**, 034003 (2022).
36. M. G. Vazimali and S. Fathpour, "Applications of thin-film lithium niobate in nonlinear integrated photonics," Adv. Photonics **4**, 034001 (2022).
37. Y. Zheng and X. Chen, "Nonlinear wave mixing in lithium niobate thin film," Adv. Phys. X **6**, 1889402 (2021).
38. Y. Qi and Y. Li, "Integrated lithium niobate photonics," Nanophotonics **9**, 1287 (2020).
39. P. A. Franken and J. F. Ward, "Optical harmonics and nonlinear phenomena," Rev. Mod. Phys. **35**, 23 (1963).
40. T. Park, H. S. Stokowski, V. Ansari, T. P. McKenna, A. Y. Hwang, M. M. Fejer, and A. H. Safavi-Naeini, "High-efficiency second harmonic generation of blue light on thin-film lithium niobate," Opt. Lett. **47**, 2706 (2022).
41. R. Luo, H. Jiang, S. Rogers, H. Liang, Y. He, and Q. Lin, "On-chip second-harmonic generation and broadband parametric down-conversion in a lithium niobate microresonator," Opt. Express **25**, 24531 (2017).
42. M. Jankowski, J. Mishra, and M. M. Fejer, "Dispersion-engineered $\chi^{(2)}$ nanophotonics: a flexible tool for nonclassical light," J. Phys. Photonics **3**, 042005 (2021).
43. R. W. Boyd, *Nonlinear Optics*, 3rd ed. (Academic Press, 2008).
44. C. Lu, Y. Zhang, J. Qiu, Y. Tang, T. Ding, S. Liu, Y. Zheng, and X. Chen, "Highly tunable birefringent phase-matched second-harmonic generation in an angle-cut lithium niobate-on-insulator ridge waveguide," Opt. Lett. **47**, 1081 (2022).
45. L. Wang, X. Zhang, and F. Chen, "Efficient second harmonic generation in a reverse-polarization dual-layer crystalline thin film nanophotonic waveguide," Laser Photonics Rev. **15**, 2100409 (2021).
46. F. Ye, Y. Yu, X. Xi, and X. Sun, "Second-harmonic generation in etchless lithium niobate nanophotonic waveguides with bound states in the continuum," Laser Photonics Rev. **16**, 2100429 (2022).
47. X. Li, J. Ma, S. Liu, P. Huang, B. Chen, D. Wei, and J. Liu, "Efficient second harmonic generation by harnessing bound states in the continuum in semi-nonlinear etchless lithium niobate waveguides," Light Sci. Appl. **11**, 317 (2022).
48. C. Wang, X. Xiong, N. Andrade, V. Venkataraman, X.-F. Ren, G.-C. Guo, and M. Lončar, "Second harmonic generation in nano-structured thin-film lithium niobate waveguides," Opt. Express **25**, 6963 (2017).
49. R. Luo, Y. He, H. Liang, M. Li, and Q. Lin, "Highly tunable efficient second-harmonic generation in a lithium niobate nanophotonic waveguide," Optica **5**, 1006 (2018).
50. R. Luo, Y. He, H. Liang, M. Li, and Q. Lin, "Semi-nonlinear nanophotonic waveguides for highly efficient second-harmonic generation," Laser Photonics Rev. **13**, 1800288 (2019).
51. A. Rao, J. Chiles, S. Khan, S. Toroghi, M. Malinowski, G. F. Camacho-González, and S. Fathpour, "Second-harmonic generation in single-mode integrated waveguides based on mode-shape modulation," Appl. Phys. Lett. **110**, 111109 (2017).
52. L. Chang, Y. Li, N. Volet, L. Wang, J. Peters, and J. E. Bowers, "Thin film wavelength converters for photonic integrated circuits," Optica **3**, 531 (2016).
53. C. Lu, H. Li, J. Qiu, Y. Zhang, S. Liu, Y. Zheng, and X. Chen, "Second and cascaded harmonic generation of pulsed laser in a lithium niobate on insulator ridge waveguide," Opt. Express **30**, 1381 (2022).
54. M. Jankowski, C. Langrock, B. Desiatov, A. Marandi, C. Wang, M. Zhang, C. R. Phillips, M. Lončar, and M. M. Fejer, "Ultrabroadband nonlinear optics in nanophotonic periodically poled lithium niobate waveguides," Optica **7**, 40 (2020).
55. A. Al Sayem, Y. Wang, J. Lu, X. Liu, A. W. Bruch, and H. X. Tang, "Efficient and tunable blue light generation using lithium niobate nonlinear photonics," Appl. Phys. Lett. **119**, 231104 (2021).
56. Y. Niu, C. Lin, X. Liu, Y. Chen, X. Hu, Y. Zhang, X. Cai, Y.-X. Gong, Z. Xie, and S. Zhu, "Optimizing the efficiency of a periodically poled LNOI waveguide using *in situ* monitoring of the ferroelectric domains," Appl. Phys. Lett. **116**, 101104 (2020).
57. J. Zhao, M. Rüsing, U. A. Javid, J. Ling, M. Li, Q. Lin, and S. Mookherjea, "Shallow-etched thin-film lithium niobate waveguides for highly-efficient second-harmonic generation," Opt. Express **28**, 19669 (2020).
58. J. Lu, M. Li, C.-L. Zou, A. Al Sayem, and H. X. Tang, "Toward 1% single-photon anharmonicity with periodically poled lithium niobate microring resonators," Optica **7**, 1654 (2020).
59. A. Boes, L. Chang, M. Knoerzer, T. G. Nguyen, J. D. Peters, J. E. Bowers, and A. Mitchell, "Improved second harmonic performance in periodically poled LNOI waveguides through engineering of lateral leakage," Opt. Express **27**, 23919 (2019).
60. J. Chen, Y. Meng Sua, Z. Ma, C. Tang, Z. Li, and Y. Huang, "Efficient parametric frequency conversion in lithium niobate nanophotonic chips," OSA Contin. **2**, 2914 (2019).
61. X. Wu, L. Zhang, Z. Hao, R. Zhang, R. Ma, F. Bo, G. Zhang, and J. Xu, "Broadband second-harmonic generation in step-chirped periodically poled lithium niobate waveguides," Opt. Lett. **47**, 1574 (2022).
62. L. Ge, Y. Chen, H. Jiang, G. Li, B. Zhu, Y. Liu, and X. Chen, "Broadband quasi-phase matching in a MgO:PPLN thin film," Photonics Res. **6**, 954 (2018).
63. D. V. Strekalov, A. A. Savchenkov, A. B. Matsko, and N. Yu, "Efficient upconversion of subterahertz radiation in a high-*Q* whispering gallery resonator," Opt. Lett. **34**, 713 (2009).
64. L. Ma, O. Slattery, and X. Tang, "Single photon frequency up-conversion and its applications," Phys. Rep. **521**, 69 (2012).
65. G. Li, Y. Chen, H. Jiang, and X. Chen, "Broadband sum-frequency generation using d_{33} in periodically poled $LiNbO_3$ thin film in the telecommunications band," Opt. Lett. **42**, 939 (2017).
66. J. Lin, N. Yao, Z. Hao, J. Zhang, W. Mao, M. Wang, W. Chu, R. Wu, Z. Fang, L. Qiao, W. Fang, F. Bo, and Y. Cheng, "Broadband quasi-phase-matched harmonic generation in an on-chip monocrystalline lithium niobate microdisk resonator," Phys. Rev. Lett. **122**, 173903 (2019).
67. S. Liu, Y. Zheng, and X. Chen, "Cascading second-order nonlinear processes in a lithium niobate-on-insulator microdisk," Opt. Lett. **42**, 3626 (2017).
68. X. Ye, S. Liu, Y. Chen, Y. Zheng, and X. Chen, "Sum-frequency generation in lithium-niobate-on-insulator microdisk via modal phase matching," Opt. Lett. **45**, 523 (2020).
69. Z. Hao, J. Wang, S. Ma, W. Mao, F. Bo, F. Gao, G. Zhang, and J. Xu, "Sum-frequency generation in on-chip lithium niobate microdisk resonators," Photonics Res. **5**, 623 (2017).
70. R. Wolf, I. Breunig, H. Zappe, and K. Buse, "Cascaded second-order optical nonlinearities in on-chip micro rings," Opt. Express **25**, 29927 (2017).
71. M. Wang, N. Yao, R. Wu, Z. Fang, S. Lv, J. Zhang, J. Lin, W. Fang, and Y. Cheng, "Strong nonlinear optics in on-chip coupled lithium niobate microdisk photonic molecules," New J. Phys. **22**, 073030 (2020).
72. A. Savchenkov, E. Lopez, I. Solomatine, D. Eliyahu, A. Matsko, and L. Maleki, "Spectral purity improvement in flickering self-injection locked lasers," IEEE J. Quantum Electron. **58**, 2200209 (2022).
73. J. Wang, B. Zhu, Z. Hao, F. Bo, X. Wang, F. Gao, Y. Li, G. Zhang, and J. Xu, "Thermo-optic effects in on-chip lithium niobate microdisk resonators," Opt. Express **24**, 21869 (2016).
74. J. Zhang, Z. Fang, J. Lin, J. Zhou, M. Wang, R. Wu, R. Gao, and Y. Cheng, "Fabrication of crystalline microresonators of high quality factors with a controllable wedge angle on lithium niobate on insulator," Nanomaterials **9**, 1218 (2019).
75. R. Zhuang, J. He, Y. Qi, and Y. Li, "High-*Q* thin-film lithium niobate microrings fabricated with wet etching," Adv. Mater. **35**, 2208113 (2023).
76. R. Wu, J. Zhang, N. Yao, W. Fang, L. Qiao, Z. Chai, J. Lin, and Y. Cheng, "Lithium niobate micro-disk resonators of quality factors above 10^7," Opt. Lett. **43**, 4116 (2018).
77. R. Gao, N. Yao, J. Guan, L. Deng, J. Lin, M. Wang, L. Qiao, W. Fang, and Y. Cheng, "Lithium niobate microring with ultra-high *Q* factor above 10^8," Chin. Opt. Lett. **20**, 011902 (2022).

78. J. Mishra, T. P. McKenna, E. Ng, H. S. Stokowski, M. Jankowski, C. Langrock, D. Heydari, H. Mabuchi, M. M. Fejer, and A. H. Safavi-Naeini, "Mid-infrared nonlinear optics in thin-film lithium niobate on sapphire," Optica **8**, 921 (2021).
79. T. Umeki, M. Asobe, O. Tadanaga, H. Takara, Y. Miyamoto, and H. Takenouchi, "Phase sensitive amplifiers based on PPLN waveguides for optical communication," in *12th International Conference on Optical Internet 2014 (COIN)* (2014), p. 1.
80. T. Kobayashi, S. Shimizu, M. Nakamura, T. Umeki, T. Kazama, R. Kasahara, F. Hamaoka, M. Nagatani, H. Yamazaki, T. Mizuno, H. Nosaka, and Y. Miyamoto, "Wideband inline-amplified WDM transmission using PPLN-based OPA with over-10-THz bandwidth," in *Optical Fiber Communications Conference and Exhibition (OFC)* (2020), paper Th4C.7.
81. Á. D. Szabö, V. Ribeiro, V. Gordienko, F. Ferreira, C. Gaur, and N. Doran, "Verification of signal-to-crosstalk measurements for WDM fiber optical parametric amplifiers," in *Conference on Lasers and Electro-Optics* (2020), paper JTu2E.1.
82. Y. Sun, H. Tu, S. You, C. Zhang, Y.-Z. Liu, and S. A. Boppart, "Detection of weak near-infrared optical imaging signals under ambient light by optical parametric amplification," Opt. Lett. **44**, 4391 (2019).
83. W. Zhao, J. Yang, J. Zhang, W. Wang, T. Zhang, L. Han, D. Cui, Q. Peng, and Z. Xu, "Efficient optical image amplifier using periodically poled lithium niobate," Appl. Opt. **54**, 9172 (2015).
84. S. Kumar, A. E. Willner, D. Gurkan, K. R. Parameswaran, and M. M. Fejer, "All-optical half adder using an SOA and a PPLN waveguide for signal processing in optical networks," Opt. Express **14**, 10255 (2006).
85. L. Eldada, "Optical communication components," Rev. Sci. Instrum. **75**, 575 (2004).
86. X. Xu, M. Tan, B. Corcoran, J. Wu, A. Boes, T. G. Nguyen, S. T. Chu, B. E. Little, D. G. Hicks, R. Morandotti, A. Mitchell, and D. J. Moss, "11 TOPS photonic convolutional accelerator for optical neural networks," Nature **589**, 44 (2021).
87. J. Feldmann, N. Youngblood, M. Karpov, H. Gehring, X. Li, M. Stappers, M. Le Gallo, X. Fu, A. Lukashchuk, A. S. Raja, J. Liu, C. D. Wright, A. Sebastian, T. J. Kippenberg, W. H. P. Pernice, and H. Bhaskaran, "Parallel convolutional processing using an integrated photonic tensor core," Nature **589**, 52 (2021).
88. M. V. Chekhova and Z. Y. Ou, "Nonlinear interferometers in quantum optics," Adv. Opt. Photonics **8**, 104 (2016).
89. R. Schnabel, "Squeezed states of light and their applications in laser interferometers," Phys. Rep. **684**, 1 (2017).
90. N. Volet, A. Spott, E. J. Stanton, M. L. Davenport, L. Chang, J. D. Peters, T. C. Briles, I. Vurgaftman, J. R. Meyer, and J. E. Bowers, "Semiconductor optical amplifiers at 2.0-μm wavelength on silicon," Laser Photonics Rev. **11**, 1600165 (2017).
91. J. Riemensberger, N. Kuznetsov, J. Liu, J. He, R. N. Wang, and T. J. Kippenberg, "A photonic integrated continuous-travelling-wave parametric amplifier," Nature **612**, 56 (2022).
92. Y. Liang, J. Zhou, Z. Liu, H. Zhang, Z. Fang, Y. Zhou, D. Yin, J. Lin, J. Yu, R. Wu, M. Wang, and Y. Cheng, "A high-gain cladded waveguide amplifier on erbium doped thin-film lithium niobate fabricated using photolithography assisted chemo-mechanical etching," Nanophotonics **11**, 1033 (2022).
93. Z. Chen, Q. Xu, K. Zhang, W.-H. Wong, D.-L. Zhang, E. Y.-B. Pun, and C. Wang, "Efficient erbium-doped thin-film lithium niobate waveguide amplifiers," Opt. Lett. **46**, 1161 (2021).
94. Q. Luo, C. Yang, Z. Hao, R. Zhang, D. Zheng, F. Bo, Y. Kong, G. Zhang, and J. Xu, "On-chip erbium-doped lithium niobate waveguide amplifiers [Invited]," Chin. Opt. Lett. **19**, 060008 (2021).
95. Y. M. Sua, J.-Y. Chen, and Y.-P. Huang, "Ultra-wideband and high-gain parametric amplification in telecom wavelengths with an optimally mode-matched PPLN waveguide," Opt. Lett. **43**, 2965 (2018).
96. T. Kishimoto, K. Inafune, Y. Ogawa, H. Sasaki, and H. Murai, "Highly efficient phase-sensitive parametric gain in periodically poled $LiNbO_3$ ridge waveguide," Opt. Lett. **41**, 1905 (2016).
97. T. Kazama, T. Umeki, S. Shimizu, T. Kashiwazaki, K. Enbutsu, R. Kasahara, Y. Miyamoto, and K. Watanabe, "Over-30-dB gain and 1-dB noise figure phase-sensitive amplification using a pump-combiner-integrated fiber I/O PPLN module," Opt. Express **29**, 28824 (2021).
98. L. Ledezma, R. Sekine, Q. Guo, R. Nehra, S. Jahani, and A. Marandi, "Intense optical parametric amplification in dispersion-engineered nanophotonic lithium niobate waveguides," Optica **9**, 303 (2022).
99. C. E. Rüter, K. Hasse, F. Chen, and D. Kip, "Optical characterization of a neodymium-doped lithium-niobate-on-insulator (LNOI)," Opt. Mater. Express **11**, 4007 (2021).
100. Q. Luo, C. Yang, Z. Hao, R. Zhang, R. Ma, D. Zheng, H. Liu, X. Yu, F. Gao, F. Bo, Y. Kong, G. Zhang, and J. Xu, "Integrated ytterbium-doped lithium niobate microring lasers," Opt. Lett. **47**, 1427 (2022).
101. S. Shimizu, T. Kobayashi, T. Kazama, T. Umeki, M. Nakamura, K. Enbutsu, T. Kashiwazaki, R. Kasahara, K. Watanabe, and Y. Miyamoto, "PPLN-based optical parametric amplification for wideband WDM transmission," J. Light. Technol. **40**, 3374 (2022).
102. M. A. Foster, A. C. Turner, J. E. Sharping, B. S. Schmidt, M. Lipson, and A. L. Gaeta, "Broad-band optical parametric gain on a silicon photonic chip," Nature **441**, 960 (2006).
103. C. Op de Beeck, B. Haq, L. Elsinger, A. Gocalinska, E. Pelucchi, B. Corbett, G. Roelkens, and B. Kuyken, "Heterogeneous III-V on silicon nitride amplifiers and lasers via microtransfer printing," Optica **7**, 386 (2020).
104. E. A. Kittlaus, H. Shin, and P. T. Rakich, "Large Brillouin amplification in silicon," Nat. Photonics **10**, 463 (2016).
105. V. Sih, S. Xu, Y.-H. Kuo, H. Rong, M. Paniccia, O. Cohen, and O. Raday, "Raman amplification of 40 Gb/s data in low-loss silicon waveguides," Opt. Express **15**, 357 (2007).
106. M. Jankowski, N. Jornod, C. Langrock, B. Desiatov, A. Marandi, M. Lončar, and M. M. Fejer, "Quasi-static optical parametric amplification," Optica **9**, 273 (2022).
107. L. Ledezma, A. Roy, L. Costa, R. Sekine, R. Gray, Q. Guo, R. Nehra, R. M. Briggs, and A. Marandi, "Octave-spanning tunable parametric oscillator in nanophotonics," arXiv.2203.11482 (2022).
108. Y. Wu, S. Liang, Q. Fu, L. Xu, and D. J. Richardson, "Compact picosecond mid-IR PPLN OPO with controllable peak powers," OSA Contin. **3**, 2741 (2020).
109. C. Xi, P. Wang, X. Li, and Z. Liu, "Highly efficient continuous-wave mid-infrared generation based on intracavity difference frequency mixing," High Power Laser Sci. Eng. **7**, e67 (2019).
110. N. Amiune, D. N. Puzyrev, V. V. Pankratov, D. V. Skryabin, K. Buse, and I. Breunig, "Optical-parametric-oscillation-based $\chi^{(2)}$ frequency comb in a lithium niobate microresonator," Opt. Express **29**, 41378 (2021).
111. P. Jiang, C. Hu, T. Chen, P. Wu, B. Wu, R. Wen, and Y. Shen, "High power Yb fiber laser with picosecond bursts and the quasi-synchronously pumping for efficient midinfrared laser generation in optical parametric oscillator," IEEE Photon. J. **8**, 1501807 (2016).
112. P. Wang, X. Cheng, X. Li, and X. Xu, "Tunable dual-wavelength, continuous-wave, mid-infrared generation using intracavity difference frequency mixing in PPLN-based optical parametric oscillator," IEEE J. Sel. Top. Quantum Electron. **24**, 0902807 (2018).
113. R. Gao, H. Zhang, F. Bo, W. Fang, Z. Hao, N. Yao, J. Lin, J. Guan, L. Deng, M. Wang, L. Qiao, and Y. Cheng, "Broadband highly efficient nonlinear optical processes in on-chip integrated lithium niobate microdisk resonators of Q-factor above 10^8," New J. Phys. **23**, 123027 (2021).
114. C. Yan, S. Wang, S. Zhao, Y. Huang, H. Zhou, G. Deng, S. Wang, and S. Zhou, "Efficient and temperature-tunable second-harmonic generation in a thin film lithium niobate on insulator microdisk," Appl. Phys. Lett. **122**, 103504 (2023).
115. R. Wolf, Y. Jia, S. Bonaus, C. S. Werner, S. J. Herr, I. Breunig, K. Buse, and H. Zappe, "Quasi-phase-matched nonlinear optical frequency conversion in on-chip whispering galleries," Optica **5**, 872 (2018).
116. J. Lu, J. B. Surya, X. Liu, A. W. Bruch, Z. Gong, Y. Xu, and H. X. Tang, "Periodically poled thin-film lithium niobate microring resonators with a second-harmonic generation efficiency of 250,000%/W," Optica **6**, 1455 (2019).
117. T. P. McKenna, H. S. Stokowski, V. Ansari, J. Mishra, M. Jankowski, C. J. Sarabalis, J. F. Herrmann, C. Langrock, M. M. Fejer, and A. H. Safavi-Naeini, "Ultra-low-power second-order nonlinear optics on a chip," Nat. Commun. **13**, 4532 (2022).
118. M. Zhang, B. Buscaino, C. Wang, A. Shams-Ansari, C. Reimer, R. Zhu, J. M. Kahn, and M. Lončar, "Broadband electro-optic frequency comb

generation in a lithium niobate microring resonator," Nature **568**, 373 (2019).
119. Y. Hu, M. Yu, B. Buscaino, N. Sinclair, D. Zhu, R. Cheng, A. Shams-Ansari, L. Shao, M. Zhang, J. M. Kahn, and M. Lončar, "High-efficiency and broadband on-chip electro-optic frequency comb generators," Nat. Photonics **16**, 679 (2022).
120. A. Shams-Ansari, M. Yu, Z. Chen, C. Reimer, M. Zhang, N. Picqué, and M. Lončar, "Thin-film lithium-niobate electro-optic platform for spectrally tailored dual-comb spectroscopy," Commun. Phys. **5**, 88 (2022).
121. K. Zhang, W. Sun, Y. Chen, H. Feng, Y. Zhang, Z. Chen, and C. Wang, "A power-efficient integrated lithium niobate electro-optic comb generator," Commun. Phys. **6**, 17 (2023).
122. Z. Fang, S. Haque, S. Farajollahi, H. Luo, J. Lin, R. Wu, J. Zhang, Z. Wang, M. Wang, Y. Cheng, and T. Lu, "Polygon coherent modes in a weakly perturbed whispering gallery microresonator for efficient second harmonic, optomechanical, and frequency comb generations," Phys. Rev. Lett. **125**, 173901 (2020).
123. L. Chang, S. Liu, and J. E. Bowers, "Integrated optical frequency comb technologies," Nat. Photonics **16**, 95 (2022).
124. Z. Gong, M. Shen, J. Lu, J. B. Surya, and H. X. Tang, "Monolithic Kerr and electro-optic hybrid microcombs," Optica **9**, 1060 (2022).
125. C. Wang, M. Zhang, M. Yu, R. Zhu, H. Hu, and M. Lončar, "Monolithic lithium niobate photonic circuits for Kerr frequency comb generation and modulation," Nat. Commun. **10**, 978 (2019).
126. Y. Okawachi, M. Yu, B. Desiatov, B. Y. Kim, T. Hansson, M. Lončar, and A. L. Gaeta, "Chip-based self-referencing using integrated lithium niobate waveguides," Optica **7**, 702 (2020).
127. R. Ikuta, M. Asano, R. Tani, T. Yamamoto, and N. Imoto, "Frequency comb generation in a quadratic nonlinear waveguide resonator," Opt. Express **26**, 15551 (2018).
128. L. Zhou, X. Wang, L. Lu, and J. Chen, "Integrated optical delay lines: a review and perspective [Invited]," Chin. Opt. Lett. **16**, 101301 (2018).
129. D. J. Moss, R. Morandotti, A. L. Gaeta, and M. Lipson, "New CMOS-compatible platforms based on silicon nitride and Hydex for nonlinear optics," Nat. Photonics **7**, 597 (2013).
130. X. Liu, S. Gao, C. Zhang, Y. Pan, R. Ma, X. Zhang, L. Liu, Z. Xie, S. Zhu, S. Yu, and X. Cai, "Ultra-broadband and low-loss edge coupler for highly efficient second harmonic generation in thin-film lithium niobate," Adv. Photonics Nexus **1**, 016001 (2022).
131. Z. Ye, P. Zhao, K. Twayana, M. Karlsson, V. Torres-Company, and P. A. Andrekson, "Overcoming the quantum limit of optical amplification in monolithic waveguides," Sci. Adv. **7**, eabi8150 (2021).
132. M. Zhang, C. Wang, R. Cheng, A. Shams-Ansari, and M. Lončar, "Monolithic ultra-high-*Q* lithium niobate microring resonator," Optica **4**, 1536 (2017).
133. A. Boes, L. Chang, T. Nguyen, G. Ren, J. Bowers, and A. Mitchell, "Efficient second harmonic generation in lithium niobate on insulator waveguides and its pitfalls," J. Phys. Photonics **3**, 012008 (2021).
134. E. Saitoh, Y. Kawaguchi, K. Saitoh, and M. Koshiba, "A design method of lithium niobate on insulator ridge waveguides without leakage loss," Opt. Express **19**, 15833 (2011).
135. S. Molesky, Z. Lin, A. Y. Piggott, W. Jin, J. Vucković, and A. W. Rodriguez, "Inverse design in nanophotonics," Nat. Photonics **12**, 659 (2018).